Dalton Transactions

Cite this: *Dalton Trans.*, 2012, **41**, 1312

www.rsc.org/dalton

PAPER

Neutral cuprous complexes as ratiometric oxygen gas sensors†

Xiaohui Liu,[a,c] Wei Sun,[a,c] Luyi Zou,[a] Zhiyuan Xie,[a] Xiao Li,*[a] Canzhong Lu,[b] Lixiang Wang[a] and Yanxiang Cheng*[a]

Received 19th September 2011, Accepted 24th October 2011
DOI: 10.1039/c1dt11777g

Four neutral mononuclear Cu(I) complexes, [Cu(pyin)(PPh_3)$_2$] (**1a**), [Cu(pyin)(DPEphos)] (**1b**), [Cu(quin)(PPh_3)$_2$] (**2a**) and [Cu(quin)(DPEphos)] (**2b**) (Hpyin = 2-(2-pyridyl)indole, Hquin = 2-(2-quinolyl)indole and DPEphos = bis(2-(diphenylphosphino)phenyl)ether) have been synthesized. X-Ray crystal structure analysis revealed that the central Cu(I) ion in all complexes is in a distorted tetrahedral coordination environment. All four complexes display the typical metal-to-ligand charge transfer (MLCT) absorption band at 371, 363, 413 and 402 nm, respectively. No emission was observed from any complexes in the solid state due to triplet–triplet annihilation. However, the complexes show unusual dual-emission originating from intraligand charge-transfer (ILCT) and MLCT transitions, when dispersed in a rigid matrix (*e.g.* PMMA) or in frozen CH_2Cl_2. The oxidation potential of Cu(I)/Cu(II) in these neutral complexes, ~0.5 V (*vs.* Ag/AgCl), is lower than those of cationic Cu(I) complexes. Films containing 10 wt% of these complexes in PMMA shows ratiometric fluorescent oxygen gas sensing property with a response ratio of 0.3–3.2 and response time of 3–4 s. Complex **2b** acts as a ratiometric oxygen gas sensor with good reversibility through energy and electron transfer mechanisms under the loss of a counteranion.

Introduction

The determination of oxygen levels is necessary in many fields, such as industrial production, environmental surveillance, medical analysis and in daily life due to its importance as an active species in these processes. Generally, oxygen detection methods are divided into chemical systems, such as the Clark electrode and chemiluminescence,[1] and physical measurement. In contrast to the chemical methods, the physical ones, such as optical sensors, can be used in wider areas and have a long-lived lifetime and good reproducibility because no reactions occur, although they are at the high level of cost as instrumental analytical methods.[2] A large number of luminescent compounds, especially recently reported phosphorescent complexes, offer more chances to improve the measuring ability of optical sensors.

Luminescent transition metal complexes should be more suitable oxygen gas sensors than organic dyes because these complexes usually show strong phosphorescent characteristics and oxygen molecules are always in the triplet ground state,[3] which are advantageous for triplet–triplet annihilation. Noble-metal complexes such as of Ru(II) or Ir(III),[4] can act as oxygen gas sensors with high sensitivity, reversibility and specificity. In particular, inexpensive Cu(I) complexes have also been applied in oxygen gas sensing because they possess analogous MLCT transitions to Ru(II) complexes.[5] However, the square-planar geometry in excited states for ionic Cu(I) complexes means that they are easily attacked by nucleophilic reagents from the environment, including counter-anions, which results in non-radiative decay, decreased emission quantum yield and sensitivity.[6] One of the improvement methods is to synthesize heteroleptic Cu(I) complexes containing a large counter-anion with low nucleophilicity. Such cationic Cu(I) complexes show excellent sensing ability to molecular oxygen,[5c] even better than Ru(II) complexes. However, a better alternative, we suggest, is to develop neutral Cu(I) complexes, which can completely avoid this effect of the counter-anion.[6]

The previous work we reported recently has demonstrated that neutral Cu(I) complexes possess a similar luminescent performance to ionic ones, based on completely identical skeletons, and are more effective phosphorescent emitters.[7] However, both the neutral and ionic complexes can simply interconvert from one to another in the presence of acid or base. Therefore, "pure" neutral Cu(I) complexes are expected to be superior potential

[a]*State Key Laboratory of Polymer Physics and Chemistry, Changchun Institute of Applied Chemistry, Chinese Academy of Sciences, Changchun, 130022, P. R. China. E-mail: xiaoli@ciac.jl.cn, yanxiang@ciac.jl.cn; Fax: +86-431-85262572; Tel: +86-431-85262106*
[b]*State Key Laboratory of Structural Chemistry, Fujian Institute of Research on the Structure of Matter, Chinese Academy of Sciences, Fuzhou, 350002, P. R. China*
[c]*The Graduate School, Chinese Academy of Sciences, Beijing, 100039, P. R. China*

† Electronic supplementary information (ESI) available: Fig. S1–S3 and crystallographic data. CCDC reference numbers CCDC 828213–828216. For ESI and crystallographic data in CIF or other electronic format see DOI: 10.1039/c1dt11777g

candidates as new phosphorescent materials. In this paper, we report four novel neutral Cu(I) complexes, in which the ligands used are 2-(2′-pyridyl)indole (Hpyin)[8] and 2-(2′-quinolyl)indole (Hquin) as well as auxiliary triphenylphosphine (PPh_3) and bis(2-(diphenylphosphino)phenyl) ether (DPEphos). Unlike the ligands used in the previous work, Hpyin or Hquin is the sole heterocyclic ligand used to prepare the present neutral Cu(I) complexes. More interestingly, these complexes were found to have oxygen gas sensing ability during the measurement of their photophysical properties.

Result and discussion

Synthesis and characterization

Scheme 1 shows the structures of four neutral Cu(I) complexes (**1a**, **1b**, **2a**, **2b**), which were readily synthesized in good yields by the elimination of NaI from the reaction of sodium salt of the ligand (Na^+pyin^- or Na^+quin^-), CuI and phosphine in the ratio of 1 : 1 : 2 under an argon atmosphere in absolute tetrahydrofuran (THF). The reactions were easily monitored by the quenching of the bright green fluorescence of the sodium salt of the ligand. Complexes **1a** and **1b** are sensitive to air in solution but are stable solids, and complexes **2a** and **2b** are relatively stable both in solution and the solid state. From thermogravimetric analysis (TGA) data, the decomposition temperatures of **1b** (362 °C) and **2b** (378 °C) (with DPEphos) are higher than that of **1a** (253 °C) and **2a** (264 °C) (with PPh_3). Hence DPEphos as an auxiliary ligand increases the thermal stability of its derived complexes.

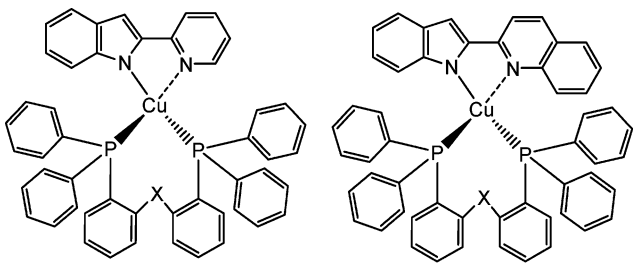

Scheme 1 The molecular structures of the complexes **1a**, **1b**, **2a** and **2b**.

Crystals of complexes **1a**, **1b**, **2a** and **2b** suitable for X-ray diffraction analysis were obtained by diffusion of methanol to the dichloromethane solution of complexes. Complexes **1a** and **1b** were obtained as yellow crystalline solids, while complexes **2a** and **2b** are red crystals. The crystallographic data are reported in Table 1, and views of the structures of the complexes **1a**, **1b**, **2a** and **2b** are shown in Fig. 1–4, respectively. Selected bond lengths and angles for complexes **1a**, **1b**, **2a** and **2b** are listed in Table 2.

X-Ray diffraction analysis shows that the Cu(I) center in all four complexes is located in a typically pseudo-tetrahedral coordination environment. Bond lengths for P–Cu, Cu–N(pyridyl or quinolyl moiety) and angles for P–Cu–P are comparable to those reported in the literature for similar heteroleptic Cu(I) complexes.[9–11] However, the bond lengths of Cu–N(indolyl moieties) (2.006–2.042 Å) are obviously shorter than those of Cu–N(pyridyl or quinolyl moieties) (2.101–2.125 Å), which indicates

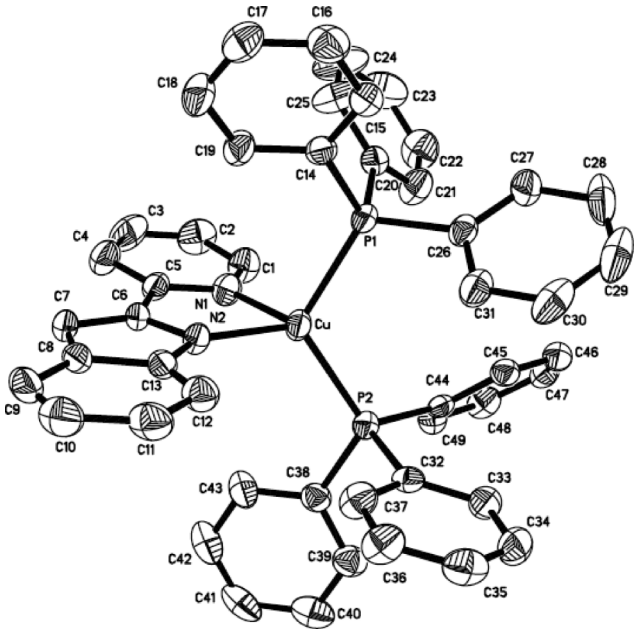

Fig. 1 Crystal structure of complex **1a** with thermal ellipsoids at 30% probability. H atoms are omitted for clarity.

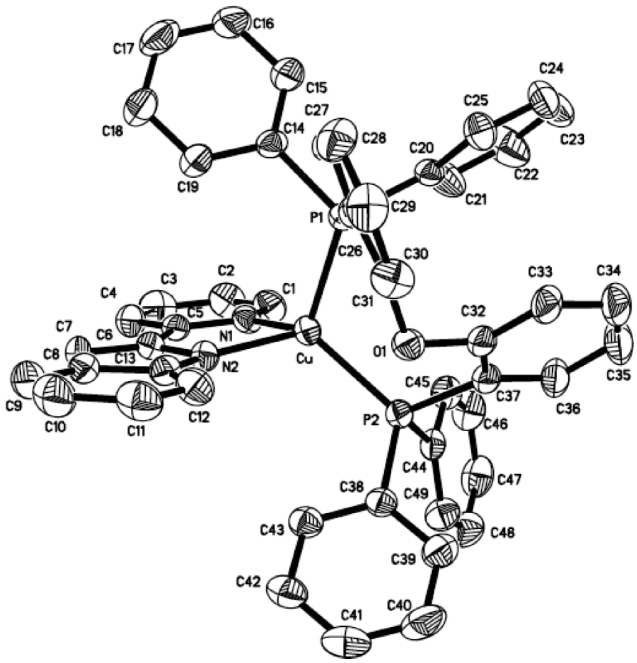

Fig. 2 Crystal structure of complex **1b** with thermal ellipsoids at 30% probability. Solvent molecules and H atoms are omitted for clarity.

that anionic indolyl moiety has more negative charge than the pyridyl or quinolyl moieties.[10] The dihedral angles between the N–Cu–N and the P–Cu–P planes of the four complexes are 86.36 (**1a**), 86.99 (**1b**), 84.44 (**2a**) and 85.42° (**2b**), respectively, which are in the normal range compared with that found in the mixed-ligand Cu(I) complexes of $[Cu(N,N)(P,P)]^+$ systems.[9,11] The N–Cu–N bond angles are similar in all the complexes (80.76–81.93 Å) with little variation. The P–Cu–P bond angle of **2a** (122.90°) is larger than that of **1a** (116.82°), which indicates that the steric hindrance of quinolyl in quin is greater than pyridyl in pyin. Intramolecular

Table 1 Crystallographic data for complexes **1a**, **1b**, **2a** and **2b**

Complex	[Cu(pyin)(PPh_3)$_2$] (**1a**)	[Cu(pyin)(POP)]·CH_2Cl_2 (**1b**)	[Cu(quin)(PPh_3)$_2$]·CH_2Cl_2 (**2a**)	[Cu(quin)(POP)]·CH_3OH (**2b**)
Empirical formula	$C_{49}H_{39}CuN_2P_2$	$C_{49}H_{37}CuN_2OP_2\cdot CH_2Cl_2$	$C_{53}H_{41}CuN_2P_2\cdot CH_2Cl_2$	$C_{53}H_{39}CuN_2OP_2\cdot CH_3OH$
M_r	781.30	880.21	916.28	877.38
Crystal system	Orthorhombic	Triclinic	Triclinic	Triclinic
Space group	$Pna2_1$	$P\bar{1}$	$P\bar{1}$	$P\bar{1}$
a/Å	20.386(3)	9.586(4)	10.9902(8)	11.7152(9)
b/Å	21.293(3)	11.370(4)	12.2055(8)	12.1017(9)
c/Å	9.1912(11)	20.412(8)	19.3749(13)	16.7936(12)
α/°		96.330(7)	75.6690(10)	74.3790(10)
β/°		93.891(7)	81.1440(10)	77.3600(10)
γ/°		103.119(7)	66.0970(10)	70.7180(10)
V/Å^3	3989.6(9)	2143.5(14)	2297.9(3)	2142.1(3)
Z	4	2	2	2
D_c/g cm^{-3}	1.301	1.364	1.324	1.360
μ/mm^{-1}	0.664	0.749	0.700	0.630
$2\theta_{max}$/°	52.12	52.30	51.44	52.10
No. reflns measd	21912	12192	12689	12056
No. reflns used	7863	8309	8560	8233
R_{int}	0.0656	0.0363	0.0206	0.0301
No. params	487	523	550	558
$R1$,[a] $wR2$[b] [$I > 2\sigma(I)$]	0.0581, 0.0896	0.0695, 0.1498	0.0549, 0.1441	0.0634, 0.1519
$R1$,[a] $wR2$[b] (all data)	0.1003, 0.1030	0.1275, 0.1819	0.0719, 0.1595	0.0899, 0.1707
GOF on F^2	1.006	1.001	1.003	1.003

[a] $R_1 = \sum[|F_o| - |F_c|]/\sum|F_o|$. [b] $wR_2 = \{\sum[w(F_o^2 - F_c^2)]/\sum(wF_o^2)\}^{1/2}$; $w = 1/[\sigma^2(F_o^2) + (0.075P)^2]$, where $P = [\max(F_o^2, 0) + 2F_c^2]/3$.

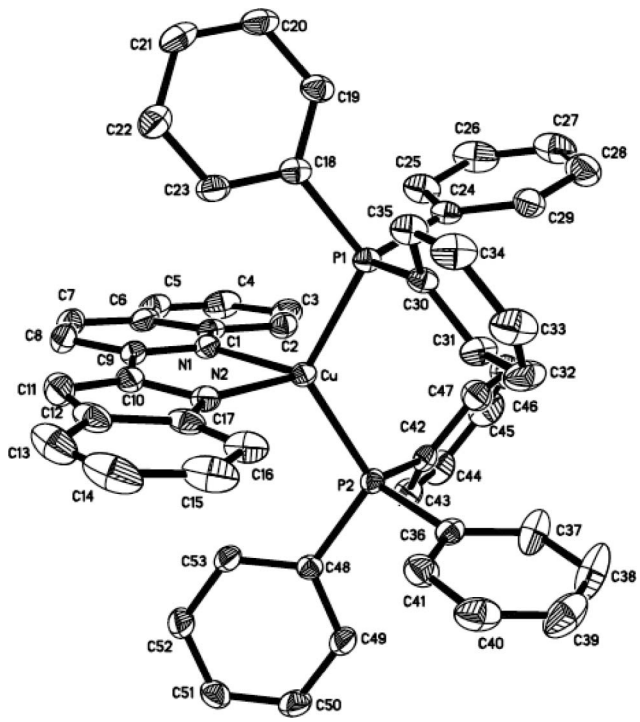

Fig. 3 Crystal structure of complex **2a** with thermal ellipsoids at 30% probability. Solvent molecules and H atoms are omitted for clarity.

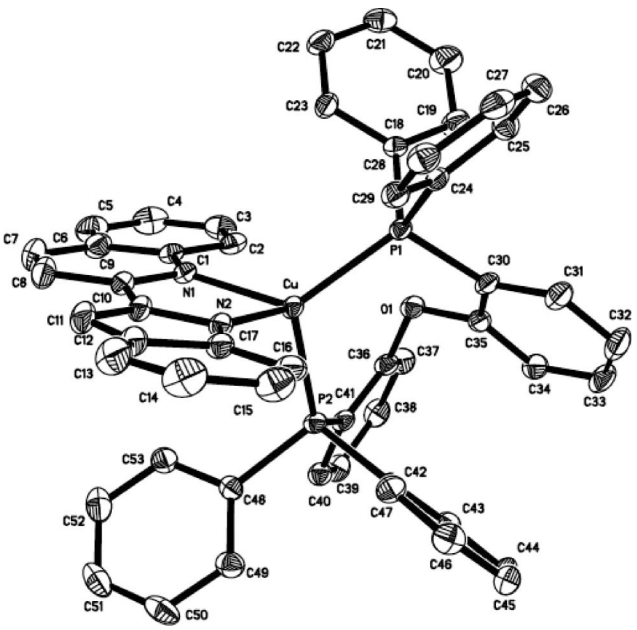

Fig. 4 Crystal structure of complex **2b** with thermal ellipsoids at 30% probability. Solvent molecules and H atoms are omitted for clarity.

π–π interactions between indolyl or quinolyl and phenyl rings (from DPEphos) of 3.455 Å (C19–N2) in **1b** and 3.423 Å (C53–N1) in **2b**, respectively, with DPEphos as the second ligand, were observed due to the restricted bite angle of the bidentate ligand,[7,12] which result in more distorted tetrahedral geometries in **1b** and **2b**. A further consequence might be the higher stability of complexes **1b** and **2b**.

Photophysical and electrochemical properties

The absorption spectra of free ligands and their corresponding complexes in CH_2Cl_2 are shown in Fig. 5 and detailed results are summarized in Table 3. These complexes exhibited weak bands at long wavelength, ranging from 350 to 450 nm for **1a** and **1b** ($\varepsilon = 5.07 \times 10^3$ and 6.69×10^3 M^{-1} cm^{-1}), and from 400 to 500 nm for **2a** and **2b** ($\varepsilon = 9.00 \times 10^3$ and 9.39×10^3 M^{-1} cm^{-1}), corresponding to electronic excitation of MLCT, in addition to intense π–π* and ILCT absorptions. It is important to note that, in the MLCT region (Fig. 5), the absorption spectra of **1b** and **2b** exhibited a

Table 2 Selected bond lengths (Å) and angles (°) for **1a**, **1b**, **2a** and **2b**

Complex	**1a**	**1b**	**2a**	**2b**
Cu–N(2)	2.017(4)	2.006(4)	2.012(3)	2.042(3)
Cu–N(1)	2.111(4)	2.112(4)	2.125(2)	2.101(3)
Cu–P(2)	2.259 (14)	2.286(16)	2.254(9)	2.311(11)
Cu–P(1)	2.244(13)	2.236(16)	2.242(9)	2.242(12)
N(2)–Cu–N(1)	81.00(15)	80.83(16)	80.76(11)	81.93(13)
N(2)–Cu–P(2)	119.64(11)	120.42(12)	116.53(8)	123.58(10)
N(1)–Cu–P(2)	113.88(12)	119.41(12)	110.67(7)	122.46(10)
N(2)–Cu–P(1)	114.96(11)	107.57(12)	105.38(8)	110.74(10)
N(1)–Cu–P(1)	103.44(12)	112.81(11)	112.90(7)	102.16(9)
P(2)–Cu–P(1)	116.82(5)	112.07(5)	122.90(3)	111.48(4)
N(1)–C(5)–C(6)–N(2)	6.7(6)	6.9(5)	–2.3(4)	–4.3(6)
N–Cu–N/P–Cu–P	86.36	86.99	84.44	85.42

Table 3 Absorbance peak (λ_{abs}, molar absorptivity) in dichloromethane; emission peak (λ_{em}), quantum yield (Φ) and lifetime (τ) of Cu(I) complexes in PMMA at 298 K

	Absorbance (DCM)	Emission (PMMA film)		
	λ_{abs}/nm, ε/M^{-1} cm^{-1}	λ_{em} (nm)	τ	Φ (%)
[Cu(pyin)-(PPh$_3$)$_2$] (**1a**)	232, 4.05×10^4 324, 1.55×10^4 371, 5.07×10^3	562 474 (weak)	1.17 μs 4.66 ns	8.0
[Cu(pyin)-(DPEphos)] (**1b**)	231, 3.24×10^4 324, 1.49×10^4 363, 6.69×10^3 414, 2.01×10^3	566 475 (weak)	1.20 μs 4.78 ns	5.0
[Cu(quin)-(PPh$_3$)$_2$] (**2a**)	231, 5.31×10^4 354, 1.56×10^4 413, 9.00×10^3	608 550 (sh)	1.32 μs 5.04 ns	4.2
[Cu(quin)-(DPEphos) (**2b**)	231, 3.81×10^4 354, 1.39×10^4 402, 9.39×10^3 463, 2.87×10^3	610 550 (sh)	1.59 μs 4.89 ns	4.4

shoulder at 414 nm ($\varepsilon = 2.01 \times 10^3$ M^{-1} cm^{-1}) and 463 nm ($\varepsilon = 2.87 \times 10^3$ M^{-1} cm^{-1}) (that was not obvious for **1a** and **2a**), which may be assigned to the ^{3}MLCT charge transition,[13] indicating that these neutral Cu(I) complexes (**1a**, **1b**, **2a** and **2b**) could possess different photophysical properties relative to the classical cationic complexes.

No emission was observed for all complexes in the solid state at ambient temperature because of triplet–triplet annihilation, but they showed emission when they were dispersed in a rigid matrix (10 wt% in PMMA, Fig. 6). The maximum emission peak of complexes **1a**, **1b**, **2a** or **2b** are at 562, 566, 608 or 610 nm, respectively, with the efficiency from 4.4–8.0% in PMMA at 298 K. The main peak is assigned to the emission from the MLCT excited state based on the large Stokes shift, while the weak feature at ~470 nm (**1a** and **1b**) or shoulder at ~550 nm (**2a** and **2b**) is presumed to be the emission originated from the ILCT transition in the pyin or quin ligands at 298 K. In order to confirm this hypothesis, the emission spectra of complex **2b**, as a typical example, were measured as a function of temperature (Fig. 7). The intensity of the short wavelength emission decreased and eventually vanished with decreasing temperature, accompanied

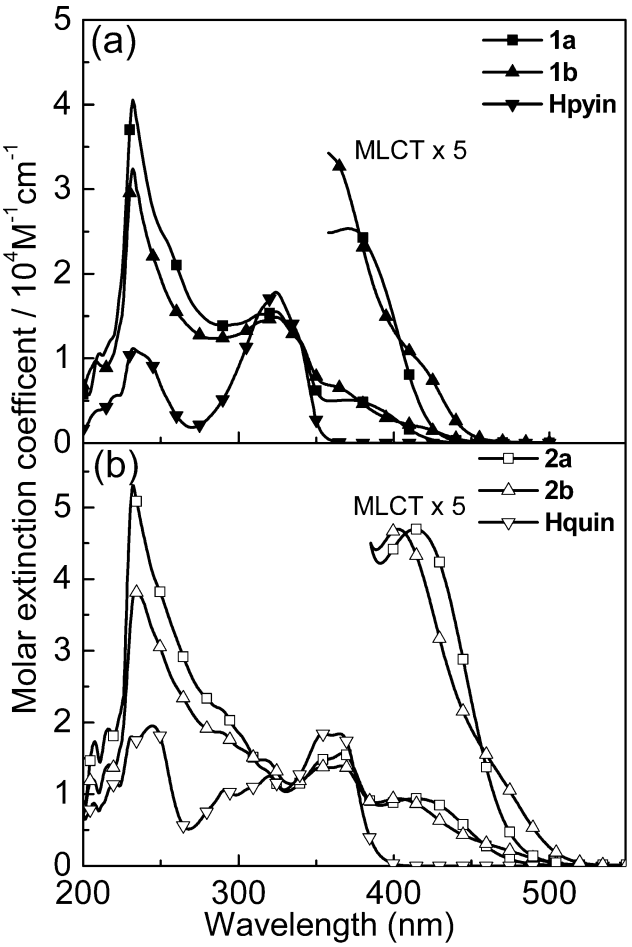

Fig. 5 Room-temperature electronic absorption spectra of complexes **1a**, **1b** with their free ligand Hpyin (a) and complexes **2a**, **2b** with their free ligand Hquin (b) in degassed CH_2Cl_2.

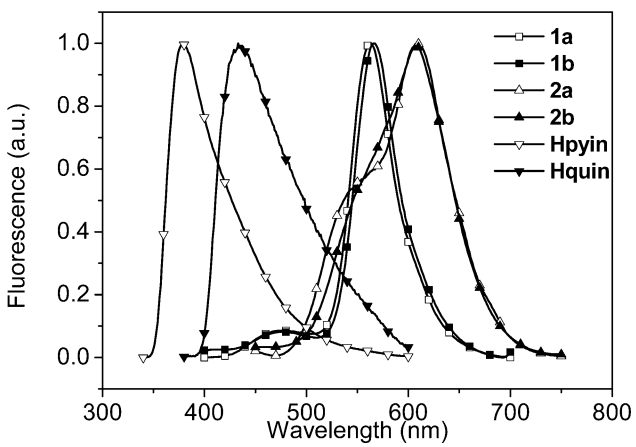

Fig. 6 The emission spectra of **1a**, **1b**, **2a** and **2b** in 10 wt% PMMA films at 298 K; λ_{ex} = 365 nm.

with an increase of the main peak emission and slight blue shift from 610 to 600 nm, since the low temperature restricted vibration of the chromophore. The short wavelength emission still persisted and exhibited the same temperature dependence even at a lower concentration of 0.5 wt% in PMMA or in a polystyrene (PS) or polycarbonate (PC) matrix at 298 K. Conclusive evidence was

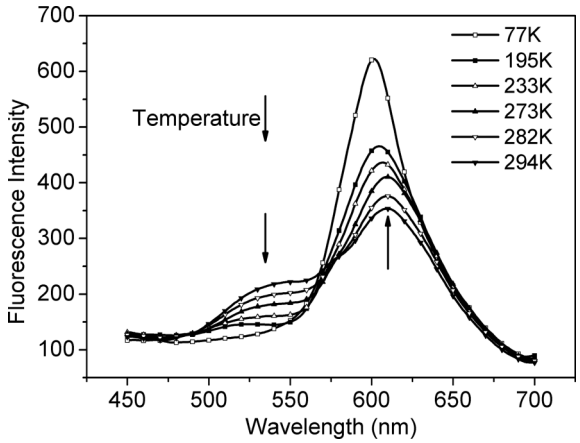

Fig. 7 Emission spectra of complex **2b** in PMMA as a function of temperature from 294 to 77 K; λ_{ex} = 365 nm.

based on the emission from the sodium salts of the ligands (Fig. S1 and S2, ESI†), which displayed similar emissive positions of shoulders and broad features as the complexes. DFT calculations also demonstrate that the emission involves MLCT and ILCT mechanisms (Fig. 8). This is the first time that dual emission in mononuclear Cu(I) complexes has been observed, although similar phenomena were reported for Ru(II),[14] Pt(II),[15] and dinuclear Cu(I)[16] complexes.

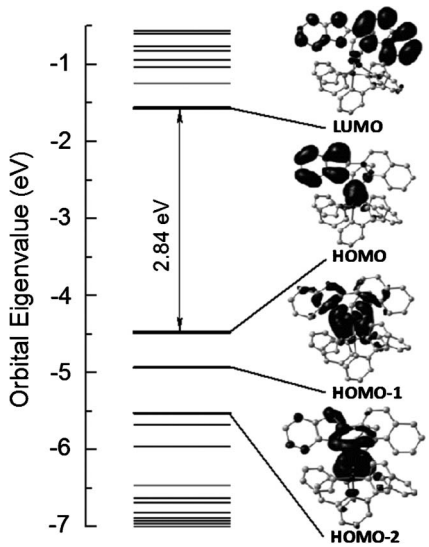

Fig. 8 Partial Kohn–Sham orbital energy-level diagram of **2b** from density functional theory (DFT) calculation.

The electrochemical behavior of the complexes was investigated by cyclic voltammetry (CV). Relative to the ionic Cu(I) complexes,[17] these neutral complexes in degassed CH_2Cl_2 solution displayed a lower irreversible oxidation peak at 0.55 (**1a**), 0.45 (**1b**), 0.60 (**2a**) and 0.51 V (**2b**), respectively (Ag/AgCl as reference), which is attributed to the oxidation of Cu(I) to Cu(II). The unusual oxidation potentials probably originate from the strong electron-donating effect of anionic indole units, which significantly increase the electron density on the Cu(I) center and hence raise the highest occupied molecular orbital (HOMO) energy level. In CH_3CN, no obvious reduction peak was observed, which indicates that the electron-rich Cu(I) center also raises the lowest unoccupied molecular orbital (LUMO) energy level of the neutral complexes. DFT calculations support this interpretation, in which the HOMO of **2b** is localized both on the indole moiety and the copper center, while HOMO–1 is distributed over the metal centered orbital; even the HOMO–2 orbital is also mainly copper-centered. The band gaps obtained from DFT calculations (3.40, 3.26, 2.78 and 2.84 eV for **1a**, **1b**, **2a** and **2b**, respectively) are consistent with the experimental MLCT absorption band (the optical band gap using the edge of the lowest-energy absorption band was determined to be 2.92, 2.77, 2.55 and 2.40 eV for complexes **1a**, **1b**, **2a** and **2b**, respectively). The relatively low oxidation potential of each Cu(I) complex readily results in combination with an oxidant, such as oxygen.[18] Thus, these neutral Cu(I) complexes exhibit a useful oxygen-sensing feature.

Molecular oxygen sensing

The oxygen gas-sensing experiments were performed on dispersions of the complexes into PMMA. Fig. 9 shows the emission spectra of a PMMA film containing a loading level of 10 wt% of complex **2b** under several different oxygen concentrations in argon, ranging from 375 to 700 nm after excitation at 365 nm. The emission from MLCT of complex **2b** with its maximum at 610 nm was easily quenched by oxygen; this was simultaneously accompanied by a fluorescence increase at 410 nm corresponding to emission from the ligand centered (LC) state of the free ligand quin (Fig. S1 and S2, ESI†). The ratios of emission intensities at λ = 411 and 610 nm ranged from 0.3 to 3.2, indicating that this complex acts as a ratiometric sensor for oxygen gas-sensing. Furthermore, the clear change of emission color from orange to blue upon excitation of UV light is desirable for ratiometric fluorescent probes, and was easily visible. Response time and relative fluorescence intensity changes of complex **2b** are recorded in Fig. 10 upon repeatedly switching environments between vacuum and 100% oxygen. Two different steps on the recovery curve by vacuum show that the removal of oxygen absorbed on the surface of a film was facile, but difficult when it was incorporated in a polymer film. The Stern–Volmer curve, fitted by

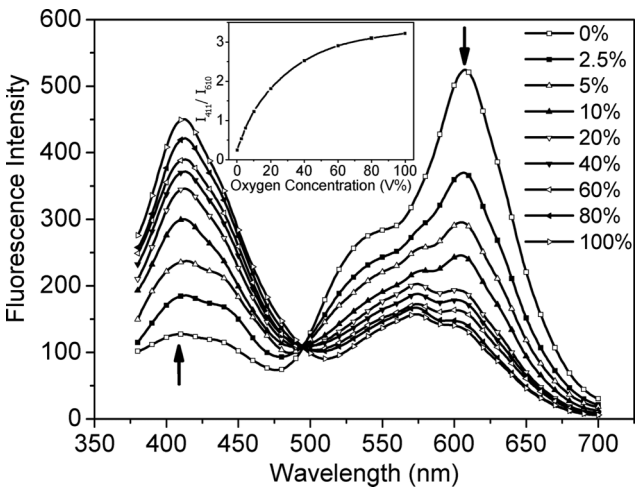

Fig. 9 Emission spectra of complex **2b** under different oxygen concentrations, λ_{ex} = 365 nm. The inset shows the ratiometric calibration curve $I_{411\,nm}/I_{610\,nm}$ as a function of oxygen concentration.

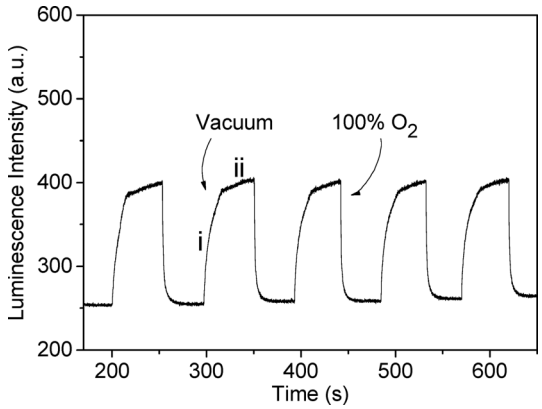

Fig. 10 Response time and relative fluorescence intensity changes at 610 nm for complex **2b** in PMMA coating upon switching between vacuum and oxygen repeatedly, λ_{ex} = 365 nm.

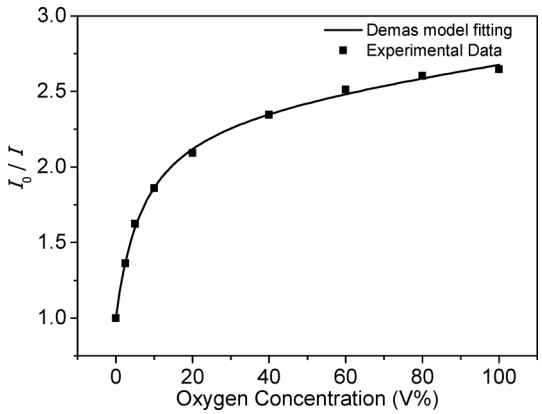

Fig. 11 Stern–Volmer plots for 10 wt% **2b** doped sample in PMMA under various oxygen concentrations from 0 to 100% at 298 K. Solid line is fitted using the Demas model: $I_0/I = [f_{01}/(1 + K_{SV1}[O_2]) + f_{02}/(1 + K_{SV2}[O_2])]^{-1}$; ($f_{01} + f_{02} = 1$), $I_0/I_{100} = 2.65$, K_{SV1} ($O_2V\%^{-1}$) = 0.33547, K_{SV2} (O_2 vol%$^{-1}$) = 0.00139, $f_{01} = 0.59393$, $f_{01} = 0.40607$, $R^2 = 0.99922$.

the Demas model, was nonlinear (Fig. 11),[19] which also shows that the complex molecules were in varying microenvironments with heterogeneous active sites originating from the depth variation of the complex molecules in the PMMA film due to the coating process.[20] The four complexes all showed a rapid response time at 3–4 s in reducing their intensity by 95% response; however, only compound **2b** displayed perfect reversibility under reduced pressure or in a flow of inert gas. Its high reproducibility is ascribed to the stronger coordination ability of the quin and the bidentate phosphine ligands relative to the other three complexes as well as to the absence of a counteranion.

Unlike the ionic Cu(I) complexes, in which only the quenching of the MLCT emission is observed as a result of the energy transfer,[3] the appearance of a high energy emissive peak indicates that dissociation of the ligand, or decomposition of the complex, might have occurred.[4] However, the rapid recovery of the MLCT emission remains unexplained. The intensity of the ILCT emission (Fig. 9) decreased more slowly than that of MLCT, and remained stronger than triplet emission, which confirms that emissions, including from LC, ILCT and MLCT transitions, are from a single molecule and share similar excitation energy. The sole difference is that of their relative intensity ratio. Thus, we suggest that this is due to charge transfer from the anionic ligand to an oxygen molecule (except for energy transfer when sensing), as shown in Fig. 12, although no direct experimental evidence is available. Some indirect information, however, supports the above postulate: (1) the sample after O_2-sensing still exhibited an MLCT absorption band (Fig. S3, ESI†), attributed to the presence of the Cu–N bond (from the pyridine ring); (2) the blue emission is proposed to originate mainly from the contribution of the indole moieties, based on the near identical emissive position of both the free ligands Hbyin and Hquin; thus the cleavage of Cu–N (indole) bond may have occurred giving rise to the indole radical; (3) DFT calculations also show that the ILCT transition increases when the MLCT transition still remains after the central Cu(I) ion is attacked by gaseous oxygen (Fig. 13). (4) The excellent reversibility for oxygen gas-sensing proves that no Cu–O bond is formed during these procedures.[20] In addition, the neutral Cu(I) complex does not contain any counter-anion, which always attacks a Cu(I) ion in the excited states as a nucleophilic reagent so inhibiting the recovery of its excited state geometry from square-planar.[6] So the neutral Cu(I) complexes readily recover their tetrahedral geometry after removal of oxygen molecules with concomitant loss of the counteranion. Hence, the mechanism should incorporate both charge and energy transfer, resulting in the formation of a radical.

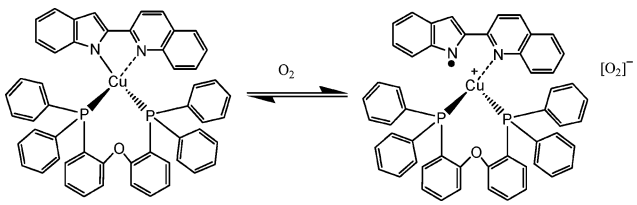

Fig. 12 The possible sensing mechanism of complex **2b** towards O_2.

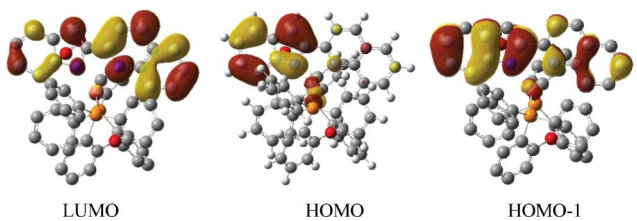

Fig. 13 LUMO, HOMO and HOMO–1 orbitals of **2b**$^+$$(O_2)^-$.

Conclusion

In summary, we have reported the first example of neutral heteroleptic Cu(I) complexes based on indole derivatives as oxygen gas sensors. These neutral Cu(I) complexes exhibit a ILCT and MLCT (singlet and triplet) dual emission from a single complex molecule. The enriched electronic density of neutral complexes ligated to the negative ligands results in atypically low oxidation potential in contrast to cationic Cu(I) complexes. The high oxygen concentration-dependent luminescence quenching property, in conjunction with a remarkable enhancing of blue fluorescence emission, makes these complexes plausible candidates as ratiometric oxygen sensors. The sensing ability obviously correlates with the rigidity of the complex molecule and the absence of counterion. The sensing mechanism of these neutral molecules is

attributed to the synergetic effect of the energy and charge transfer. Further studies to develop new neutral Cu(I) complexes with high photoluminescent quantum yields, by improving the rigidity of the anionic ligands, are in progress.

Experimental

General

Starting materials were purchased from Sigma–Aldrich, Acros or Fluka and used without further purification. Solvents were freshly distilled over appropriate drying reagents under an argon atmosphere. All experiments were carried out under a dry argon atmosphere using standard Schlenk techniques unless otherwise stated.

Characterization. ^{1}H NMR and ^{13}C NMR with TMS as internal reference and ^{31}P NMR spectra with 85% H_3PO_4 as external reference were recorded on a Bruker Avance 600 MHz spectrometer at room temperature. Elemental analyses for C, H and N were performed with a BioRad elemental analysis system. Thermogravimetric analysis (TGA) was performed on a Perkin–Elmer series 7 analysis systems under N_2 at a heating rate of 10 °C min^{-1}. Absorption spectra were recorded on a Perkin–Elmer Lambda35 UV/Vis Spectrometer. Photoluminescence spectra were recorded on SHIMADZU RF-5301PC Spectrofluorophotometer. The measurements at low temperature (77 K) were performed in quartz tubes inserted in a liquid-nitrogen-filled quartz Dewar. The HOMO and LUMO energies were determined using XRD geometries to approximate the ground state. The PL quantum yields were determined by the integrating sphere with 409 nm excitation of a HeCd laser. Luminescence lifetimes were measured with a Lecroy Wave Runner 6100 digital oscilloscope (1 GHz) using a tunable laser (pulse width = 4 ns, gate = 50 ns) for the excitation (Continuum Sunlite OPO). The samples for all the steady optical spectra were in sealed quartz cuvettes under nitrogen atmosphere. Cyclic voltammetry was performed using a on Chi660b electrochemical ananlyzer with a three-electrode cell in 0.1 M tetrabutylammonium perchlorate (Bu_4NClO_4), in dry dichloromethane solution under an argon atmosphere at a scan rate of 100 mV s^{-1} and using ferrocene as standard, in which a glassy carbon working electrode, a Pt auxiliary electrode, and a Ag/AgCl reference electrode were employed.

The films for oxygen sensing was made as follows: 5 mg Cu(I) complex and 45 mg PMMA (MW = 12 000) powder were dissolved in 0.5 ml absolute dichloromethane under an argon atmosphere, then the viscous mixture solution was filmed and dried on the wall of a cylindrical cuvette by gradual vacuum avoiding bubbles. The cuvette was fixed on a modified appurtenance in the darkroom of luminescence spectrometer, and a tube was piped between the cuvette and the pressure system. Oxygen sensitivity was measured by monitoring the fluorescence intensity of the coating film upon switching between vacuum and certain oxygen concentration in the quartz cuvette.

X-Ray crystallography. The crystal data was collected on a Bruker Smart APEX diffractometer with CCD detector and graphite monochromated Mo-Kα radiation (λ = 0.71073 Å). The intensity data were recorded with ω scan mode (298 K). Lorentz polarization factors were made for the intensity data and absorption corrections were performed using SADABS program.[21] The crystal structure was solved using the SHELXTL program and refined using full-matrix least squares.[22] All non-hydrogen atoms were refined anistropically. The positions of the hydrogen atoms attached to carbon atoms were fixed at their ideal positions. The crystallographic data are reported in Table 1.

DFT calculations were performed using GAUSSIAN 03 W software package using a spin-restricted formalism at the B3LYP level. The basis sets 6-311++G** was used for all other atoms.[23]

Synthesis

[Cu(pyin)(PPh_3)$_2$] (1a). A typical procedure is as follows. A degassed mixture of ligand Hpyin (0.194 g, 1.0 mmol) and NaH (0.12 g, 5.0 equiv.) were stirred in 10 ml newly evaporated THF for 2 h under an argon atmosphere in flask A. CuI (0.190 g, 1.0 mmol) and triphenylphosphine (0.532 g, 2.0 mmol) were degassed, and stirred in 10 ml THF for 2 h under the argon atmosphere in flask B. The solution of sodic ligand in flask A was transferred to Cu(I) solution in flask B. The reaction mass was stirred for 2 h, then the solvent was evaporated under vacuum to dryness. The solid residue was extracted with 10 ml absolute dichloromethane under the argon atmosphere while the extract was filtered and transferred to an argon-protected flask. 10 ml methanol was layered above the resulting solution afforded yellow crystals of complex **1a**, which were washed with methanol, yield 0.65 g (84%); Mp169 °C; ^{1}H NMR (600 MHz, $CDCl_3$) δ 7.88–7.81 (m, J = 7.3 Hz, 2H), 7.67–7.63 (m, 1H), 7.50 (t, J = 7.5 Hz, 1H), 7.30–7.08 (m, 32H), 6.86–6.81 (m, 2H), 6.71 (t, J = 7.5 Hz, 1H); ^{13}C NMR (151 MHz, $CDCl_3$) δ 156.44, 148.29, 147.11, 145.46, 136.25, 134.65, 134.51, 133.66, 133.56, 132.39, 129.17, 128.38, 128.32, 120.14, 119.95, 119.59, 119.32, 117.36, 116.54, 98.75; ^{31}P NMR (243 MHz, $CDCl_3$) δ –0.75. Elemental analysis for $C_{49}H_{39}CuN_2P_2$: calc.: C, 73.83; H, 5.33; N: 3.44; found: C, 73.76; H, 5.30; N, 3.37%.

The procedures for the synthesis of **1b**, **2a** and **2b** were similar to the described as **1a**. Only the quantities of ligand that were used, the product yields, the melting points, NMR data, and elemental analyses are given.

[Cu(pyin)(DPEphos)] (1b). Using Hpyin (0.194 g, 1.0 mmol) and bis(2-(diphenylphosphino)phenyl)ether (0.538 g, 1.0 mmol) afforded 0.57 g yellow crystals of **1b** (72%). Mp 210 °C; ^{1}H NMR (600 MHz, ppm, $CDCl_3$) δ 7.86 (d, J = 4.9 Hz, 1H), 7.77 (d, J = 8.0 Hz, 1H), 7.59 (d, J = 7.6 Hz, 1H), 7.43 (t, J = 7.6 Hz, 1H), 7.27–6.95 (m, 26H), 6.88 (t, J = 7.5 Hz, 2H), 6.80–6.72 (m, 4H), 6.57 (t, J = 7.5 Hz, 1H); ^{13}C NMR (151 MHz, $CDCl_3$) δ 158.63, 156.25, 148.14, 147.18, 145.39, 135.64, 134.27, 133.69, 133.15, 133.05, 132.96, 132.20, 130.65, 128.99, 128.10, 128.07, 128.04, 126.31, 124.29, 120.20, 119.82, 119.63, 119.19, 118.62, 117.52, 116.05, 97.78; ^{31}P NMR (243 MHz, $CDCl_3$) δ –14.43. Elemental analysis for $C_{49}H_{37}CuN_2OP_2{\cdot}CH_2Cl_2$: calc.: C, 68.22; H, 4.47; N, 3.18; found: C, 68.09; H, 4.35; N, 3.06%.

[Cu(quin)(PPh_3)$_2$] (2a). Using Hquin (0.244 g, 1.0 mmol) and triphenylphosphine (0.532 g, 2.0 mmol) afforded 0.68 g red crystals of **2a** (81%). Mp 157 °C; ^{1}H NMR (600 MHz, $CDCl_3$) δ 8.00 (q, J = 8.6 Hz, 2H), 7.66 (d, J = 7.4 Hz, 1H), 7.59 (dd, J = 12.7, 8.2 Hz, 2H), 7.32 (s, 1H), 7.30–7.21 (m, 18H), 7.19 (t, J = 7.4 Hz, 1H), 7.17–7.10 (m, 12H), 7.00–6.94 (m, 2H), 6.85–6.77 (m, 2H); ^{13}C NMR (151 MHz, $CDCl_3$) δ 156.85, 148.17, 146.77, 146.53, 136.58, 135.24,

134.96, 134.22, 134.02, 132.74, 132.56, 132.44, 129.58, 129.22, 129.09, 128.83, 128.72, 127.76, 127.48, 124.98, 121.01, 120.59, 120.04, 117.99, 117.19, 102.21; ^{31}P NMR (243 MHz, $CDCl_3$) δ –0.72. Elemental analysis for $C_{53}H_{41}CuN_2P_2{\cdot}CH_2Cl_2$: calc.: C, 70.78; H, 4.73; N, 3.06; found: C, 70.57; H, 4.46; N, 2.89%.

[Cu(quin)(DPEphos)] (2b). Using Hquin (0.244 g, 1.0 mmol) and bis(2-(diphenylphosphino)phenyl)ether (0.538 g, 1.0 mmol) afforded 0.64 g of **2b** (76%). Mp 196 °C; ^{1}H NMR (600 MHz, $CDCl_3$) δ 7.90 (d, J = 8.6 Hz, 1H), 7.82 (d, J = 8.6 Hz, 1H), 7.77 (d, J = 8.4 Hz, 1H), 7.62 (d, J = 7.8 Hz, 1H), 7.52 (t, J = 8.7 Hz, 2H), 7.49–7.45 (m, 1H), 7.32 (dt, J = 23.0, 7.1 Hz, 1H), 7.22–6.85 (m, 30H), 6.84–6.79 (m, 2H), 6.70 (t, J = 7.6 Hz, 1H); ^{13}C NMR (151 MHz, $CDCl_3$) δ 158.85, 155.94, 147.68, 146.48, 146.39, 135.34, 134.32, 133.16, 132.27, 130.68, 128.99, 128.64, 127.98, 127.87, 126.96, 126.96, 126.9, 126.84, 126.73, 124.36, 124.17, 120.55, 119.82, 119.53, 119.42, 117.7, 116.14, 100.86; ^{31}P NMR (243 MHz, $CDCl_3$) δ –13.7. Elemental analysis for $C_{53}H_{39}CuN_2OP_2{\cdot}CH_3OH$: calc.: C, 73.92; H, 4.94; N, 3.19; found: C, 73.62; H, 4.76; N, 3.07%.

Acknowledgements

This work was supported by the National Natural Science Foundation of China (Nos. 20874098, 51073152 and 51073152) and the 973 Project (2009CB623600).

References

1 K. S. Johnson, J. A. Needoba, S. C. Riser and W. J. Showers, *Chem. Rev.*, 2007, **107**, 623 and references therein.
2 C. Baleizão, S. Nagl, M. Schäferling, M. N. Berberan-Santos and O. S. Wolfbeis, *Anal. Chem.*, 2008, **80**, 6449.
3 J. N. Demas and B. A. DeGraff, *Coord. Chem. Rev.*, 2001, **211**, 317.
4 (*a*) K. A. McGee and K. R. Mann, *J. Am. Chem. Soc.*, 2009, **131**, 1896; (*b*) J. F. Fernàndez-Sànchez, T. Roth, R. Cannas, Md. K. Nazeeruddin, S. Spichiger, M. Graetzel and U. E. Spichiger-Keller, *Talanta*, 2007, **71**, 242, and references therein; (*c*) Z. G. Xie, L. Q. Ma, K. E. deKrafft, A. Jin and W. B. Lin, *J. Am. Chem. Soc.*, 2010, **132**, 922; (*d*) D. E. Achatz, R. J. Meier, L. H. Fischer and O. S. Wolfbeis, *Angew. Chem., Int. Ed.*, 2011, **50**, 260.
5 (*a*) M. T. Miller and T. B. Karpishin, *Sens. Actuators, B*, 1999, **61**, 222; (*b*) Y. H. Wang, B. Lin, Y. H. Liu, L. M. Zhang, Q. H. Zuo, L. F. Shi and Z. M. Su, *Chem. Commun.*, 2009, 5868; (*c*) C. S. Smith, C. W. Branham, B. J. Marquardt and Kent R. Mann, *J. Am. Chem. Soc.*, 2010, **132**, 14079.
6 A. Lavie-Cambot, M. Cantuel, Y. Leydet, G. Jonusauskas, D. M. Bassani and N. D. McClenaghan, *Coord. Chem. Rev.*, 2008, **252**, 2572.
7 J. H. Min, Q. S. Zhang, W. Sun, Y. X. Cheng and L. X. Wang,, *Dalton Trans.*, 2011, **40**, 686.
8 S. F. Liu, Q. G. Wu, H. L. Schmider, H. Aziz, N. X. Hu, Z. Popović and S. N. Wang, *J. Am. Chem. Soc.*, 2000, **122**, 3671.
9 S. M. Kuang, D. G. Cuttell, D. R. McMillin, P. E. Fanwick and R. A. Walton, *Inorg. Chem.*, 2002, **41**, 3313.
10 T. McCormick, W. L. Jia and S. N. Wang, *Inorg. Chem.*, 2006, **45**, 147.
11 D. G. Cuttell, S. M. Kuang, P. E. Fanwick, D. R. McMillin and R. A. Walton, *J. Am. Chem. Soc.*, 2002, **124**, 6.
12 N. Armaroli, G. Accorsi, G. Bergamini, P. Ceroni, M. Holler, O. Moudam, C. Duhayon, B. Delavaux-Nicot and J. F. Nierengarten, *Inorg. Chim. Acta*, 2007, **360**, 1032.
13 G. B. Shaw, C. D. Grant, H. Shirota, E. W. Castner, G. J. Meyer and L. X. Chen, *J. Am. Chem. Soc.*, 2007, **129**, 2147.
14 (*a*) L. Q. Song, J. Feng, X. S. Wang, J. H. Yu, Y. J. Hou, P. H. Xie, B. W. Zhang, J. F. Xiang, X. C. Ai and J. P. Zhang, *Inorg. Chem.*, 2003, **42**, 3393; (*b*) T. E. Keyes, C. O'Connor and J. G. Vos, *Chem. Commun.*, 1998, 889; (*c*) E. C. Glazer, D. Magde and Y. Tor, *J. Am. Chem. Soc.*, 2005, **127**, 4190.
15 Z. M. Hudson, S. B. Zhao, R. Y. Wang and S. N. Wang, *Chem.–Eur. J.*, 2009, **15**, 6131.
16 (*a*) K. Matsumoto, N. Matsumoto, A. Ishii, T. Tsukuda, M. Hasegawa and T. Tsubomura, *Dalton Trans.*, 2009, 6795; (*b*) W. F. Fu, X. Gan, C. M. Che, Q. Y. Cao, Z. Y. Zhou and N. Y. Zhu, *Chem.–Eur. J.*, 2004, **10**, 2228.
17 J. R. Bacon and J. N. Demas, *Anal. Chem.*, 1987, **59**, 2780.
18 J. N. Demas, B. A. Degraff and W. Y. Xu, *Anal. Chem.*, 1995, **67**, 1377.
19 (*a*) L. F. Shi and B. Li, *Eur. J. Inorg. Chem.*, 2009, 2294; (*b*) L. F. Shi, B. Li, S. Z. Lu, D. X. Zhu and W. L. Li, *Appl. Organomet. Chem.*, 2009, **23**, 379.
20 (*a*) S. Herres-Pawlis, G. Berth, V. Wiedemeier, L. Schmidt, A. Zrenner and H.-J. Warnecke, *J. Lumin.*, 2010, **130**, 1958; (*b*) L. M. Mirica, X. Ottenwaelder and T. D. P. Stack, *Chem. Rev.*, 2004, **104**, 1013; (*c*) E. A. Lewis and W. B. Tolman,, *Chem. Rev.*, 2004, **104**, 1047; (*d*) H. R. Lucas, G. J. Meyer and K. D. Karlin, *J. Am. Chem. Soc.*, 2010, **132**, 12927.
21 R. H. Blessing, *Acta Crystallogr., Sect. A: Found. Crystallogr.*, 1995, **51**, 33–38.
22 S. G. M. Sheldrick, *Version 5.1*, Bruker Analytical X-ray Systems: Inc. Madison, WI, 1997; K. A. McGee, B. J. Marquardt and K. R. Mann, *Inorg. Chem.*, 2008, **47**, 9143–9145.
23 M. J. Frisch, G. W. Trucks, H. B. Schlegel, G. E. Scuseria, M. A. Robb, J. R. Cheeseman, J. A. Montgomery, Jr., T. Vreven, K. N. Kudin, J. C. Burant, J. M. Millam, S. S. Iyengar, J. Tomasi, V. Barone, B. Mennucci, M. Cossi, G. Scalmani, N. Rega, G. A. Petersson, H. Nakatsuji, M. Hada, M. Ehara, K. Toyota, R. Fukuda, J. Hasegawa, M. Ishida, T. Nakajima, Y. Honda, O. Kitao, H. Nakai, M. Klene, X. Li, J. E. Knox, H. P. Hratchian, J. B. Cross, V. Bakken, C. Adamo, J. Jaramillo, R. Gomperts, R. E. Stratmann, O. Yazyev, A. J. Austin, R. Cammi, C. Pomelli, J. Ochterski, P. Y. Ayala, K. Morokuma, G. A. Voth, P. Salvador, J. J. Dannenberg, V. G. Zakrzewski, S. Dapprich, A. D. Daniels, M. C. Strain, O. Farkas, D. K. Malick, A. D. Rabuck, K. Raghavachari, J. B. Foresman, J. V. Ortiz, Q. Cui, A. G. Baboul, S. Clifford, J. Cioslowski, B. B. Stefanov, G. Liu, A. Liashenko, P. Piskorz, I. Komaromi, R. L. Martin, D. J. Fox, T. Keith, M. A. Al-Laham, C. Y. Peng, A. Nanayakkara, M. Challacombe, P. M. W. Gill, B. G. Johnson, W. Chen, M. W. Wong, C. Gonzalez and J. A. Pople, *GAUSSIAN 03 (Revision A.9)*, Gaussian, Inc., Wallingford, CT, 2004.